Heliyon 6 (2020) e05309

Contents lists available at ScienceDirect

Heliyon

journal homepage: www.cell.com/heliyon

Research article

Adsorption of lead ions from wastewater using nano silica spheres synthesized on calcium carbonate templates

Milton Manyangadze [a], Nyaradzai M.H. Chikuruwo [b], T. Bala Narsaiah [c], Ch. Shilpa Chakra [c], Gratitude Charis [d], Gwiranai Danha [d], Tirivaviri A. Mamvura [d,*]

[a] Chemical and Process Systems Engineering Department, Harare Institute of Technology, Harare, Zimbabwe
[b] Industial and Manufacturing Engineering Department, Harare Institute of Technology, Harare, Zimbabwe
[c] Institute of Chemical Sciences and Technology, Jawaharlal Nehru Technological University, Hyderabad, India
[d] Department of Chemical, Materials and Metallurgical Engineering, College of Engineering and Technology, Botswana International University of Science and Technology, Plot 10071, Boseja Ward, Private Bag 16 Palapye, Botswana

ARTICLE INFO

Keywords:
Chemical engineering
Environmental science
Physical chemistry
Environmental chemical engineering
Adsorption
Surface chemistry
Environmental pollution
Nano sodium silicate hollow spheres
Equilibrium studies
Freundlich isotherm
Langmuir isotherm
Thermodynamic studies
Wastewater
Lead ions

ABSTRACT

Lead is a heavy metal that is bio accumulative and non-biodegradable that poses a threat to our health when it exists in excess in our bloodstream. It has found its way into wastewater from mostly chemical industrial processes. In this article, we investigated the adsorption and hence removal of lead (II) ions from wastewater in order to purify it for re-use in industrial processes or for plant and animal use. We synthesized nano silica hollow spheres (NSHS) and used them as adsorbents to remove lead ions from wastewater. When we characterized the NSHS using X-Ray diffraction, the amorphous nature of silica was evident with average crystal size of 39.5 nm. Scanning electron microscopy was used to determine the morphology of the adsorbent and the particles were found to be spherical in shape within a size range of 100–200 nm. Thermogravimetric analysis was used to determine the mass loss of NSHS which was ~2% at 800 °C. Our experimental results from adsorption studies showed that there was a linear relationship between temperature (27–60 °C) and adsorption efficiency and an inverse relationship between initial metal concentration (50–300 mg/L) and adsorption efficiency. At a maximum temperature of 60 °C and maximum initial metal concentration of 300 mg/L, the adsorption capacity was 200 mg/g and 262 mg/g, respectively while the adsorption efficiency was 99.6% and 87.4%, respectively. Our equilibrium and thermodynamic results revealed that the process was better modelled by the Langmuir adsorption isotherm (q_{max} = 266.89 mg/g and b = 0.89 L/mg). The adsorption process was both endothermic (ΔH = 97 kJ/mol) and spontaneous (ΔG = -22 kJ/mol). We can conclude that we were able to successfully synthesize NSHS, use them to remove lead (II) ions and the produced NSHS have a capacity that is higher than most other adsorbents investigated by other researchers.

1. Introduction

One of the socio-economic challenges we face in the present day world is access to fresh water for human consumption and industrial purposes. Our fauna and flora especially in Southern Africa have also succumbed to the diminishing levels of this basic natural resource (Sayago et al., 2020). Global warming increase in small and medium enterprises (SMEs), absence of child birth policies, persistent droughts and over population (Singh et al., 2013) are amongst many other factors, that have contributed to this challenge, mainly in Africa. This is mostly due to pollution of water and/or water bodies sometimes from wastewater. There are four classes of pollutants in wastewater; namely organic, inorganic, heavy metals and alkaline earth metals, and pathogens (Huang and Chen, 2009; Singh et al., 2011). Pollution of water bodies from heavy metal and alkaline earth metal ions mainly from chemical industries has also contributed to this challenge of water shortage. Examples of chemical industries that have contributed to heavy metal pollution include tanneries, battery manufacturing, textiles, paints and dyes, and metal plating (Badruddoza et al., 2013; Gusain et al., 2019; Hao et al., 2012; Mohammadifard and Amiri, 2017). Heavy metal and alkaline earth ions like lead and zinc, respectively, have been proven to be carcinogenic and cause health disorders in humans and aquatic life.

* Corresponding author.
E-mail addresses: mamvurat@biust.ac.bw, atmamvura@gmail.com (T.A. Mamvura).

https://doi.org/10.1016/j.heliyon.2020.e05309
Received 19 May 2020; Received in revised form 7 August 2020; Accepted 15 October 2020

This is because they are highly toxic, bio-accumulative and non-biodegradable (Li et al., 2020). The presence of metal ions like lead, arsenic and chromium in potable water and/or wastewater, has been associated with different cancers like skin cancer, lung cancer, kidney cancer among others (Li et al., 2020). Besides being carcinogenic, metals like lead and chromium have also been reported as potential teratogens as well as mutagens (Sayago et al., 2020). Lead is also highly toxic and it has been linked to various health problems like brain damage, mental disturbances, retardation and reduction in the production of haemoglobin. It also affects vital internal body parts such as the reproductive system, nervous system, and is associated with problems of high blood pressure and anaemia (Hao et al., 2012). Because of all these prior listed challenges, governments and environmentalists have come up with stringent measures aimed at monitoring and reducing heavy metal concentration levels from industrial effluents. This approach has resulted in a lot of research effort being directed towards the development of new and improved technologies that can significantly handle heavy metals and reduce their concentration to below the stipulated disposal limits. Hence, we elucidate that the novelty aspect in our studies in this manuscript lie on the ejection of lead ions from wastewater by way of adsorption on silica nano spheres that we synthesized on calcium carbonate templates.

There are many different methods that can be used to remove heavy metals from wastewater like precipitation, solvent extraction, ion exchange and membrane separation but only adsorption seems to be an economical option at this stage. The application of adsorption as a unit operation in domestic water and industrial wastewater treatment processes has gained a lot of popularity in modern day plants. A lot of research has been done on adsorption of heavy metal ions over the years, but the research is still continuing. Different adsorbents have been proposed and they can be classified into different groups that include chemical adsorbents, zeolites, bio adsorbents and nano-adsorbents (Mohammadifard and Amiri, 2017). However, most proposed adsorbents have not been economical due to separation and regeneration, and so research still continues to find the ideal adsorbent for heavy metal ion removal. El-Naggar et al. (2019) investigated the adsorption of Pb^{2+} ions from wastewater using Kaolinite/Smectite natural composite adsorbents and observed positive results at pH of 2, a linear relationship between adsorption rate and temperature from 30 to 75 °C, and a linear relationship up to 100 mg/L then an inverse relationship from 100 to 500 mg/L with adsorption capacity, and their adsorption process followed Freundlich isotherm ($R^2 = 1$). Higher pH led to H^+ ions adsorption instead of Pb^{2+} ions. Mustapha et al. (2019) investigated adsorption of metal ions (Pb^{2+}, Cd^{2+}, Zn^{2+}, Cu^{2+}) from aqueous solutions using powdered adsorbent made from *Albizia lebbeck* pods. They varied different parameters and found optimum parameters of pH of 10, contact time of 30 min, lower initial metal concentration of 10 mg/L, high adsorbent dosage of 1.4 g and high temperature of 80 °C. The adsorption process was best modelled by the Langmuir isotherm model ($R^2 > 0.94$). The process was endothermic and non-spontaneous at low temperatures, but it was spontaneous at higher temperatures.

Currently, there is a growing trend in interest and demand for nano-adsorption technologies in wastewater treatment processes. Nanomaterials have gained popularity in water treatment because of their large surface area to volume ratio, and surface multi-functionality that makes them to easily react chemically and bind/adsorb a specific target metal ion(s) on their surfaces (Kegl et al., 2020; Mohammadifard and Amiri, 2017). These nano-adsorbents are employed to remove various types of pollutants from industrial wastewater. The nanomaterials can be magnetic or non-magnetic, magnetic nanomaterials can be separated using permanent magnets at the end of the adsorption process, while non-magnetic nanomaterials will require different means of separation (Kegl et al., 2019). In this study we employed non-magnetic nanomaterials. Mohammadifard and Amiri (2017) investigated the removal of Cu^{2+} ions from aqueous solutions using novel synthesized $CaCO_3$ nanoparticles prepared in a colloidal gas aphron. The adsorption process was best modelled by the Langmuir isotherm based on correlation coefficient, R^2 of 0.9999. Different parameters were optimised and using response surface methodology, they got maximum removal capacity (q_{max}) of 393.53 mg/g at 26 °C, initial Cu concentration of 200 mg/L, adsorbent dosage of 0.5 g/L, pH of 5.5 and contact time of 60 min Gusain et al. (2019) investigated adsorption of Pb^{2+} and Cd^{2+} ions from industrial mine wastewater by using hierarchical MoS_2/SH-MWCNT nanocomposite synthesized using a facile hydrothermal method and they observed good results. Optimised parameters for the process were an adsorbent dosage of 2 mg/ml, pH of 6, initial metal concentration of 45 mg/L and a temperature of 55 °C for both Pb^{2+} and Cd^{2+} ions, and contact time of 60 min for Pb^{2+} ions and 75 min for Cd^{2+} ions. Their process was better modelled by the Freundlich isotherm model ($0.86 \leq R^2 \leq 0.95$), and the process was endothermic ($\Delta H = 8.06$ kJ/mol) and spontaneous ($\Delta G \approx$ -9 kJ/mol). Nano-adsorbents are proving to be superior in terms of separation efficiency and cost as compared to adsorbents like activated carbon (Li et al., 2020). These research findings have led to nano-adsorbents being considered commercially as an economically viable, environmentally friendly and sustainable resource option during adsorption of heavy metals from wastewater (Gao et al., 2020). Within the sphere of nano adsorbents, silica-based nanomaterials are finding a lot of application and a lot of attention in water and wastewater treatment processes.

A lot of research has been done on the removal of heavy metal ions from wastewater using silica nano-particles and their derivatives as adsorbents because they have been shown to have very good properties like definite pore size, high surface area, good selectivity and adsorption capacity. However, silica is employed in its modified form, either functionalized or as a composite (Kegl et al., 2020). Generally, several different functional groups have been considered. Different researchers employed these functional groups and contributed immensely to the growing body of knowledge on this subject. Kegl et al. (2020) have shown different silica based materials that have been synthesized for adsorption studies: (a) silica functionalized nanomaterials (NMs), see their Figure 3; (b) silica/polymer nano compounds (NCs), see their Figure 4; (c) functionalized silica/compounds NCs, see their Figure 5 and (d) silica core@shell nanoparticles (NPs), see their Figure 6. All of these silicas based materials are also summarised in Table 1 in their paper. Kegl et al. (2019) investigated adsorption of dysprosium (Dy^{3+}) ions, a critical rare earth element, using novel γ-Fe_2O_3–NH_4OH@SiO_2(APTMS) nanoparticles and the process showed very good results that fit the Temkin isotherm, and the process was endothermic and spontaneous. Li et al. (2020) prepared thiol-functionalized cobalt ferrite magnetic mesoporous silica composite (SH-mSiO_2@$CoFe_2O_4$) using the modified Stöber method and used the composite to remove Hg^{2+} ions from aqueous solutions. The magnetic composite was separated using its magnetic properties after adsorption within 1 min. The composite showed very good adsorption capability with a maximum adsorption of 258 mg/g at room temperature when the initial concentration of Hg^{2+} ions was 8 mg/L. The optimum conditions were initial metal concentration of 30 mg/L, contact time of 20 min, lower temperature of 15 °C within a pH range of 2–6.

When considering adsorption of metal ions from wastewater, the most important property that we consider is a high adsorption ability, which is linked to a large surface area to volume ratio (Kegl et al., 2019). This gave us the platform to look at silica-based nano spheres supported on $CaCO_3$ as adsorbents to remove Pb^{2+} ions from wastewater. $CaCO_3$ is one of the most abundant materials found in nature (Mohammadifard and Amiri, 2017) and this justified its use as a support for silica-based nano spheres in our study. To the best of our knowledge, there is no research that has been done on nano silica spheres supported on calcium carbonate as an adsorbent for removing Pb^{2+} ions from wastewater. In this article, we focussed on the synthesis and characterization of non-metallic nano silica spheres (NSHS) with calcium carbonate ($CaCO_3$) as a template, for application in the removal of Pb^{2+} ions from industrial wastewater.

Table 1. Statistical analysis using t-test on three parameters.

Parameter	Equilibrium concentration of adsorbed metal ions (C_e)	Adsorbed metal ions per unit mass of adsorbent (q_e)	Absorption efficiency (R)
Standard value: Effect of Temperature	0	200	100%
Standard value: Effect of initial metal ion concentration	0	40, 100, 200, 300	100%

2. Experimental work

2.1. Materials

We obtained all the raw materials and samples for our experimental programme from Harare, Zimbabwe. In order for us to synthesize NSHS we used anhydrous calcium chloride (AR, $CaCl_2{\cdot}2H_2O$, 99%), anhydrous potassium carbonate (AR, K_2CO_3, 99.9%), anhydrous sodium hydroxide (AR, NaOH, 99.9%), anhydrous hydrochloric acid (AR, HCl, 36%), and deionised water (millipore).

2.2. Methods

We carried out the synthesis for NSHS in three stages, apart from the preparation of sodium silicate step. The details of this synthesis process are covered in Manyangadze et al. (2017). We then further employed three characterization methods for the analysis of NSHS, namely, X-Ray diffraction (XRD), Scanning Electron Microscopy (SEM) and Thermogravimetric Analysis (TGA). Some adsorption studies focusing on adsorption kinetics of Pb^{2+} ions were discussed in Manyangadze et al. (2017). The current work focusses primarily on the effect of temperature and initial metal ion concentration on adsorption of Pb^{2+} ions to determine equilibria data and adsorption thermodynamics.

2.3. Preparation of NSHS

We employed the sol-gel method which consists of hydrolysis, condensation, aging, and drying as highlighted in Kegl et al. (2020). Our work on adsorption of Pb^{2+} ions from aqueous solutions has not been reported as far as we can tell but Chen et al. (2004) prepared and characterized porous hollow silica nanoparticles for drug delivery application while Mourhly et al. (2015) synthesised and characterized low-cost mesoporous silica SiO_2 from local pumice rock. As such the method for synthesis of NSHS was adapted and modified from their studies. The procedure involves initially disintegrating the $CaCO_3$ template in hydrochloric acid to produce NSHS nanoparticles. We then weighed 4 g of the prepared $CaCO_3$ nanoparticles into a 500 ml beaker and added 200 ml of deionized water. We then stirred the suspension that was formed using a stirring speed of 700 rpm. While still stirring, we dropwise added 150 ml of a 0.4 M sodium silicate solution and heated the mixture to a temperature of 80 ± 1 °C for 30 min. After which, we further dropwise added a volume of 75 ml of a 2.0 M HCl acid while still stirring continuously at an increased speed between 800 and 900 rpm for an additional 40 min. We then left the mixture to cool at room temperature overnight in order to form a gel. We separated the formed gel by filtration and washed it three times using deionized water. We then dried it in an air oven set at 80 ± 1 °C for 5 h. Afterwards we took the dried solid and pulverized it in an agate mortar before the calcination process. We went on to carry out calcination at a temperature of 450 ± 1 °C for a time period of 3 h in a muffle furnace in order to produce NHSH. We proceeded to characterise the synthesized NSHS using XRD, SEM and TGA analyses. XRD was used to determine the composition of NSHS by identifying distinct peaks linked to functional groups, we used SEM to determine the morphology of the NSHS including their crystallinity and particle sizes and TGA was employed to determine any mass loss in NSHS as temperature was increased, i.e. this investigates any volatile compounds within the NSHS structure.

The structure and properties of synthesized nanomaterials are affected by the nature of precursor, solvent used, the modifying agents as well as the process conditions, such as pH and temperature (Kegl et al., 2020). However, the high purity and uniform nanostructure achievable at low temperatures made the sol-gel method attractive for synthesis of NHSH in this study.

2.4. Adsorption studies

We carried out experiments to determine the effect of initial sorbate concentration and temperature, on adsorption rates. We adopted the experimental procedure employed in this section from El-Aila et al. (2016); Kegl et al. (2019).

2.4.1. Effect of temperature

We investigated the change in adsorption rates of Pb^{2+} ions onto NHSH as a function of temperature. The experiments we carried out employed a predetermined amount of the adsorbent of 50 mg, optimum pH of 5.0, a contact time of 40 min and stirring speed of 450 rpm, as determined in Manyangadze et al. (2017). An initial sorbate concentration of 200 mg/L was used. We then suspended the adsorbent in 50 ml of sorbate solution at a pH of 5.0. We proceeded to vary the temperature from 27 ± 1 °C, 40 ± 1 °C, 50 ± 1 °C to 60 ± 1 °C. After 40 min of contact time, we filtered the samples to separate the cake adsorbent from the filtrate. The residual sorbate concentration was then analysed for lead concentration using Atomic Absorption Spectroscopy (AAS).

2.4.2. Effect of initial sorbate concentration

To enable us to investigate the effect of initial metal ion concentration on the rate of adsorption, we suspended 50 mg of the adsorbent in 50 ml of varied sorbate concentration ranging from 40, 100, 200–300 mg/L. We then fixed the stirring speed at 450 rpm, pH at 5.0, temperature at 27 ± 1 °C and a residence time of 40 min. After which, we filtered the samples to separate the cake adsorbent. We proceeded to determine the residual sorbate or equilibrium concentration using AAS. This enables us to evaluate the optimum initial sorbate concentration.

2.4.3. Adsorption isotherms

There are several adsorption isotherms available in literature, namely: Langmuir, Freundlich, BET, Temkin, Dubinin-Radushkevitch, Hill, Redlich-Peterson, and Sips (Kegl et al., 2020) but in this study we employed only two, Langmuir (equation 1) and Freundlich (equation 3) isotherms as they are the most commonly used theoretical adsorption isotherm models. These isotherms show the effect of initial concentration of metal ions and temperature on the adsorption process. We computed the adsorption capacities at equilibrium (q_e) from Eqs. (2) and (4) for Langmuir and Freundlich isotherms, respectively. To achieve this, we used 100 mL beakers to prepare 50 mL volume of Pb^{2+} ion solutions of varying concentrations, up to the optimum initial concentration of 200 mg/L. The solution pH was adjusted to the optimum value of pH 5.0 using a 0.1 M nitric acid and sodium hydroxide solutions. We proceeded to add 50 mg of the adsorbent and dispersed it by means of magnetic stirring at 450 rpm for a time period of 2 h. After equilibrium was attained, the samples were then filtered in order to separate the cake adsorbent from the filtrate. We went on to determine the residual Pb^{2+} ion concentrations by AAS in the filtrate. We then used the data generated to best fit both our models as given by Eqs. (2) and (4) as well as the

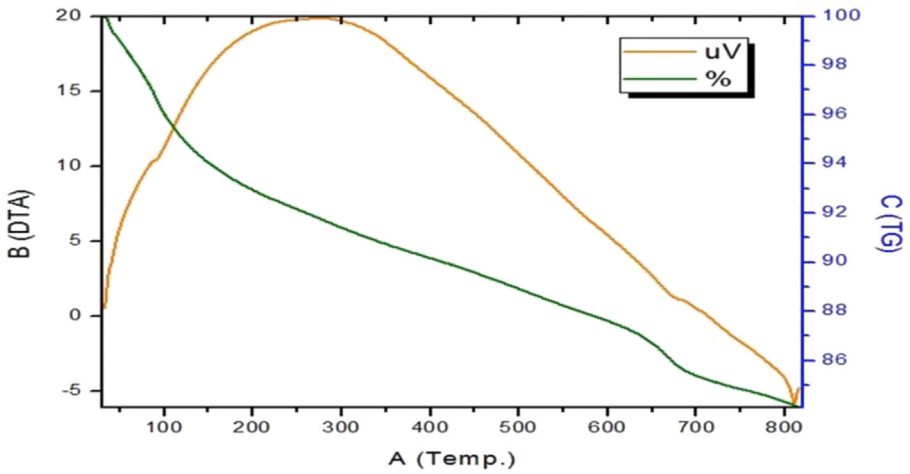

Figure 1. TG/DTA curves for NSHS particles.

equilibrium relationship, Eq. (5) (El-Aila et al., 2016; Gao et al., 2020; Kumar, 2014; Sayago et al., 2020).

Langmuir Isotherm equations

$$q_e = \frac{q_m b C_e}{1 + b C_e} \tag{1}$$

$$\frac{C_e}{q_e} = \frac{1}{q_m b} + \frac{C_e}{q_m} \tag{2}$$

Freundlich Isotherm equations

$$q_e = K_f C_e^{\frac{1}{n}} \tag{3}$$

$$\ln q_e = \ln K_f + \frac{1}{n} \ln C_e \tag{4}$$

Equilibrium relationship equation

$$q_e = \frac{(C_o - C_e)V}{W} \tag{5}$$

In the equations, q_e represents the adsorbed metal ions per unit mass of adsorbent (mg/g); q_m represents the maximum adsorbed metal ions per unit mass of adsorbent (mg/g), and this is a characteristic Langmuir parameter; b represents the Langmuir adsorption equilibrium constant and is sometimes known as K_L the equilibrium constant (L/mg); C_o represents the initial concentration of metal ions before adsorption (mg/L); C_e represents the equilibrium concentration of adsorbed metal ions (mg/L); K_f represents the adsorption capacity (L/mg); 1/n represents the adsorption intensity (g/L) which is the relative distribution of the energy and the non-homogeneity of the adsorbate sites (n is adsorption energetics), V represents the total volume of the solution that contains the Pb^{2+} ions in litres and W represents the mass of the adsorbent (g) used.

The adsorption studies can be quantified by many parameters and one of them is the adsorption efficiency, which we used in this study (Kumar, 2014; Sayago et al., 2020):

$$\%R = \frac{C_o - C_e}{C_o} \times 100 \tag{6}$$

2.4.4. Adsorption thermodynamics

Adsorption thermodynamics shows the impact of temperature on the adsorption process. The experiments we performed to investigate the

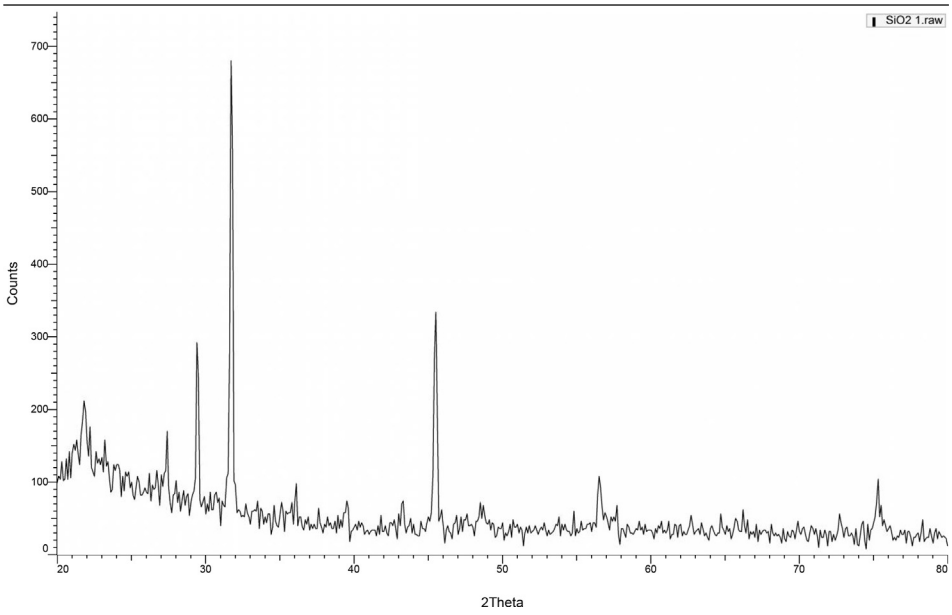

Figure 2. XRD pattern for NSHS particles.

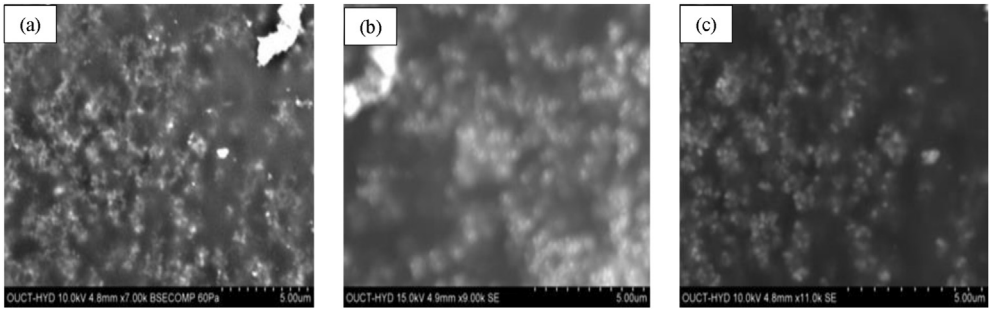

Figure 3. SEM images for NSHS particles. (a) SEM micrograph at 5μm showing spherical particles of diameter within range 100–200 nm, (b) SEM micrograph at 5μm showing particle aggregation, (c) SEM micrograph at 5μm showing particle aggregation.

effect of temperature on the adsorption rates, gave us the basis on which to evaluate the associated adsorption thermodynamics. We employed AAS to measure the concentration of the metal ions at equilibrium (C_e) in mg/L. We went on to evaluate concentration of the adsorbed metal ions (C_a) in mg/L, using Eq. (7). We calculated values for the dimensionless thermodynamic equilibrium constant (K_p) using Eq. (8). The dimensionless thermodynamic equilibrium constant was computed using the adsorption equilibrium constant as in Kegl et al. (2019) and Kegl et al. (2020) but modified to our study as Eq. (8) before computing the associated thermodynamic parameters using equations from (9, 10, 11) (El-Aila et al., 2016; El-Naggar et al., 2019; Gao et al., 2020; Kumar, 2014; Sayago et al., 2020).

$$C_a = C_o - C_e \tag{7}$$

$$K_p = \frac{K_f C_o}{\gamma} \tag{8}$$

$$\ln K_p = -\frac{\Delta G^o}{RT} \tag{9}$$

$$\Delta G^o = \Delta H^o - T\Delta S^o \tag{10}$$

$$\ln K_p = -\frac{\Delta H^o}{RT} + \frac{\Delta S^o}{R} = -\frac{\Delta G^o}{RT} \tag{11}$$

where C_a is the concentration of the adsorbed metal ion in mg/L; R is the universal gas constant; K_p is adsorption equilibrium constant which is calculated from K_L for Langmuir isotherm or K_f for Freundlich isotherm, γ is a dimensionless coefficient of activity (it is assumed as 1 as the adsorbate solution is very diluted), G is Gibbs free energy of the process (J/mol); T is the absolute temperature (K); H is enthalpy of the process (J/mol) and S is entropy of the process (J/mol·K).

The purpose of adsorption thermodynamics is to determine the if the adsorption is exothermic ($\Delta H < 0$) or endothermic ($\Delta H > 0$), spontaneous ($\Delta G < 0$) or non-spontaneous ($\Delta G > 0$) as well as to see if the metal ions like to be in random disorder ($\Delta S > 0$) or ordered on the adsorbent solid surface ($\Delta S < 0$).

2.5. Statistical analysis

We performed two forms of statistical analysis in this study. The first one was done with analysis of variance (ANOVA). During the experiments to determine the effect of temperature and initial metal ion concentration on the adsorption process, the experiments were performed three times and an average value was determined afterwards. Statistical

Table 2. Equilibrium adsorption capacity at T = 27, 40, 50 and 60 °C.

Parameter		C_o (mg/L)	W (g)	V (ml)	pH	t (mins)	Speed (rpm)	C_e (mg/L)	q_e (mg/g)
27 °C	Exp 1	200	0.05	50	5.0	40	450	49.50	150.50
	Exp 2	200	0.05	50	5.0	40	450	30.35	169.65
	Exp 3	200	0.05	50	5.0	40	450	40.90	159.10
40 °C	Exp 1	200	0.05	50	5.0	40	450	15.10	184.90
	Exp 2	200	0.05	50	5.0	40	450	25.35	174.65
	Exp 3	200	0.05	50	5.0	40	450	20.36	179.64
50 °C	Exp 1	200	0.05	50	5.0	40	450	10.46	189.54
	Exp 2	200	0.05	50	5.0	40	450	7.50	192.50
	Exp 3	200	0.05	50	5.0	40	450	7.85	192.15
60 °C	Exp 1	200	0.05	50	5.0	40	450	0.00	200.00
	Exp 2	200	0.05	50	5.0	40	450	0.00	200.00
	Exp 3	200	0.05	50	5.0	40	450	2.56	197.44

Table 3. Summary of results showing effect of temperature on adsorption capacity.

T (°C)	C_e (mg/L)	q_e (mg/g)	R	K_f (L/mg)	K_p	1/T (K^{-1})	ln K_p
27	40.25	159.75	79.88%	3.97	793.79	0.0033	6.68
40	20.27	179.73	89.87%	8.87	1773.36	0.0032	7.48
50	8.60	191.40	95.70%	22.25	4449.36	0.0031	8.40
60	0.85	199.15	99.57%	233.38	46675.00	0.0030	10.75

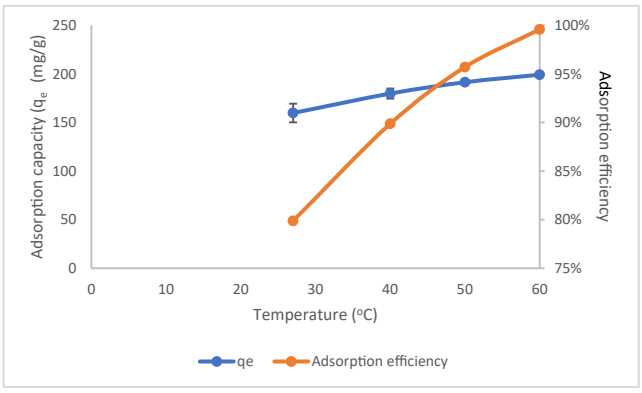

Figure 4. Effect of temperature on adsorption capacity and sorption efficiency of NSHS.

analysis using ANOVA's single factor in Microsoft Office Excel was used to determine if there was any difference between the three experimentally determined values so that we can gain confidence in the average value calculated from the three values (Dekking et al., 2005; Quirk, 2014).

The standard hypotheses for ANOVA: Single Factor for our study are (Quirk, 2014):

- Null hypothesis: All the three values from the experiments can be considered equal
- Alternative hypothesis: All the three values from the experiments can be considered significantly different

If the p-value (P-value from MS Excel) is less than our significance level which we set at 0.05, we reject the null hypothesis and conclude that the values are significantly different, meaning that their average cannot be considered reliable (Bonamente, 2017; Dekking et al., 2005; Quirk, 2014).

The second analysis was performed using Microsoft Office Excel's t-test: Paired Two Sample for Means to test if the calculated values performs well against standard values we were supposed to get. T-test was used because the sample for our experiments was small (Bonamente, 2017; Dekking et al., 2005). T-test was performed on the parameters summarised in Table 1.

The equilibrium concentration (C_e) ideally was supposed to be 0 mg/L for both cases but in reality, it was more than that. The equilibrium adsorbed metal ions (q_e) should ideally be 200 mg/g for the effect of temperature while it changes to the maximum value for the effect of initial metal ion concentration. This could only be achieved if C_e values were at their lowest expected values. In addition, adsorption efficiency ideally should be 100% to show that all metal ions have been adsorbed but in reality, it was not possible, and the t-test was meant to see if there is any significant effect from the values that we determined.

The statistical t-tests were based on the following:

(a) Do the C_e values obtained in the experiments differ very much from the standard C_e value of 0 mg/L?
(b) Do the q_e values obtained in the experiments differ very much from the standard q_e values of 200 mg/g for effect of temperature and 40, 100, 200 and 300 mg/g for effect of initial metal ion concentration?
(c) Do the R values obtained in the experiments differ very much from the standard R value of 100%?

The standard t-test uses the following hypotheses (Quirk, 2014):

- Null hypothesis: The calculated value is equal to the standard value
- Alternative hypothesis: The calculated value is not equal to the standard value

If the p-value for two tailed test (P (T<=t) two-tail from MS Excel) is less than our significance level which we set at 0.05, then we can reject the null hypothesis and conclude that the calculated values are significantly not equal to the standard values (Bonamente, 2017; Quirk, 2014).

3. Experimental results and analysis

3.1. Characterization techniques

Morphology, thermal stability and particle size are the three characterization techniques we employed to assess inherent surface characteristics of the prepared nanomaterials. These characteristics are typically relevant in understanding the ejection of heavy metals from aqueous systems. Outlined below are the results we obtained from the various analytical techniques of the NSHS.

3.1.1. Thermogravimetric analyses (TG/DTA)

Figure 1 shows a significantly low material loss for NSHS. The overall material loss is here pegged at approximately 15%. Apparently, a very low material loss is observed around 100 °C, amounting to approximately 1% and this endothermic effect is attributed to loss of physically adsorbed moisture (Mourhly et al., 2015) but it seems to stretch up to 200 °C. Other endothermic effects are observed at 650 °C with a loss of approximately 2% and at around 805 °C as shown on both the TG and DTA curves.

3.1.2. XRD analysis

Figure 2 shows XRD analysis of the NSHS particles with distinct peaks at 22°, 29.5°, 31.5°, 45°, 56.5° and 75.5° with a characteristic peak of importance appearing at $2\theta = 22^{o}$. In their work, in which SiO_2 was synthesized via neutralization reaction of sodium silicate with sulphuric acid, Music et al. (2011)located the characteristic peak at 21.8°. Misran et al. (2013); Mourhly et al. (2015) and Zulfiqar et al. (2016) indicated that the $2\theta = 22^{o}$ peak shows the presence of SiO_2 which is amorphous and that there was no crystalline structure. From the XRD pattern, the amorphous nature of silica is quite evident and using the Scherrer Eq. (12), the average crystal size was also determined and found to be 39.5 nm. The presence of $CaCO_3$ was confirmed by the characteristic peak at 29.5° as highlighted in Mohammadifard and Amiri (2017) and Zulfiqar et al. (2016).

$$d_{XRD} = \frac{K\lambda}{\beta Cos\theta} \tag{12}$$

3.1.3. SEM analysis

We employed SEM analysis to gather important information about the morphology, texture, size as well as shape of the nanoparticles. Micrograph images of NSHS nanoparticles are shown in Figure 3. The figure

Table 4. Summary of statistical analysis from studies on effect of temperature on adsorption efficiency.

Statistical test	ANOVA	t-test		
	C_e data in triplet	C_e vs minimum Ce of 0 mg/L	q_e vs maximum C_e of 200 mg/g	%R vs maximum R of 100%
p-value	0.9713	0.2212	0.2212	0.2212

Table 5. Equilibrium adsorption capacity at C_o = 27, 40, 50 and 60 °C.

Parameter		T (°C)	W (g)	V (ml)	pH	t (mins)	Speed (rpm)	C_e (mg/L)	q_e (mg/g)
40 mg/L	Exp 1	27	0.05	50	5.0	120	450	0.00	40.00
	Exp 2	27	0.05	50	5.0	120	450	0.00	40.00
	Exp 3	27	0.05	50	5.0	120	450	0.00	40.00
100 mg/L	Exp 1	27	0.05	50	5.0	120	450	0.00	100.00
	Exp 2	27	0.05	50	5.0	120	450	0.30	99.70
	Exp 3	27	0.05	50	5.0	120	450	0.80	99.20
200 mg/L	Exp 1	27	0.05	50	5.0	120	450	0.00	200.00
	Exp 2	27	0.05	50	5.0	120	450	15.10	184.90
	Exp 3	27	0.05	50	5.0	120	450	9.50	190.50
300 mg/L	Exp 1	27	0.05	50	5.0	120	450	15.12	284.88
	Exp 2	27	0.05	50	5.0	120	450	53.10	246.90
	Exp 3	27	0.05	50	5.0	120	450	45.25	254.75

Table 6. Summary of results showing effect of initial sorbate concentration on adsorption capacity.

C_o	C_e	q_e	R	C_e/q_e	$\ln q_e$	$\ln C_e$
40	0.00	40.00	100%	0.00	3.69	-
100	0.37	99.63	99.63%	0.00	4.60	-1.00
200	8.20	191.80	95.90%	0.04	5.26	2.10
300	37.82	262.18	87.39%	0.14	5.57	3.63

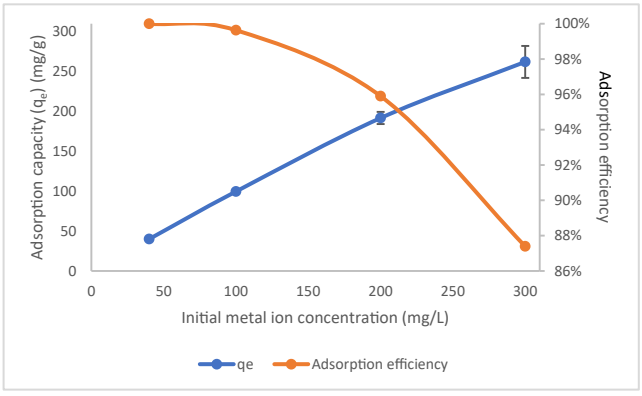

Figure 5. Adsorption isotherm for Pb^{2+} on NSHS.

reveals that the particles are mostly spherical in shape and particle aggregation is also observed. The size of the particles was found to be in the range of 100–200 nm. Also, from the micrographs, distinct particles are not clearly separated, hence the morphology of the material could not be easily ascertained.

3.2. Adsorption studies

We investigated the removal of Pb^{2+} ions using NSHS. We systematically looked at the effect of two of the various adsorption parameters, temperature and initial sorbate concentration.

3.2.1. Effect of temperature

Table 2 presents results showing the effect of temperature on the rate of adsorption and adsorption capacity, while Table 3 gives a summary of the results which are then plotted in Figure 4. Table 4 shows p-values from statistical analysis using ANOVA for C_e values in triplet, and using t-test for C_e, q_e and %R values.

Table 4 indicates that the means for C_e values range from a low of 15.800 to a high of 18.765 showing that our means are very close from ANOVA analysis. The p-value is 0.9713 which is greater than our significance level of 0.05 and therefore we accept the null hypothesis that our sample data provide strong enough evidence to conclude that the three C_e values for each temperature can be considered to be equal. This gives us the confidence that the average values we calculated and used in our calculations are a representative of the actual experimental results obtained. From t-test analysis, the mean for the actual and standard values for C_e, q_e and %R are 9.91 versus 0, 190.10 versus 200 and 0.95 versus 1, respectively. Our p-values for C_e, q_e and %R are all greater than the confidence level of 0.05 and therefore we accept the null hypothesis. Our sample data support the hypothesis that there is no significant difference between our calculated values of C_e, q_e and %R and their standard values.

Figure 4 shows a near linear relationship between temperature versus adsorption capacity as well as adsorption efficiency. It can be observed from the plot that as temperature is increased from ambient (27 °C) to 60 °C there is a corresponding increase in the adsorption capacity. For Pb^{2+} ions to be adsorbed, dehydration has to occur, and the process has to absorb heat that is availed by an increase in temperature (Lei et al., 2019). As the temperature further increases, the degree of hydration of hydrated metal ions also increases, justifying improved adsorption rates associated with higher temperatures (Lei et al., 2019). Mustapha et al. (2019) argued that the increase in adsorption capacity with an increase in temperature resulted in an increase in the mobility of the Pb^{2+} metal

Table 7. Summary of statistical analysis from studies on effect of initial metal ion concentration on adsorption efficiency.

Statistical test	ANOVA	t-test		
	C_e data in triplet	C_e vs minimum Ce of 0 mg/L	q_e vs maximum C_e of 40, 100, 200 and 300 mg/g	%R vs maximum R of 100%
p-value	0.6163	0.3080	0.3080	0.2567

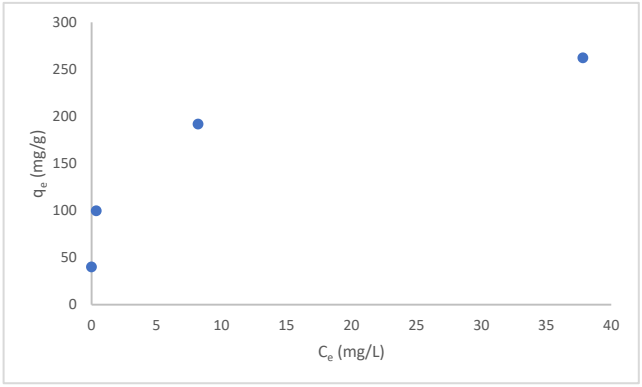

Figure 6. Adsorption isotherm for Pb^{2+} on NSHS.

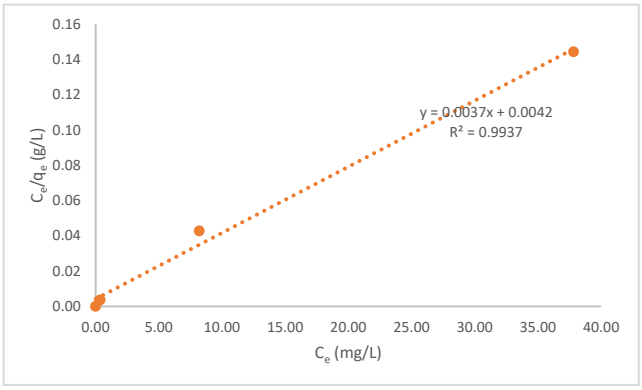

Figure 7. Linearized plot for the Langmuir isotherm model.

ions as they acquired more kinetic energy due to increased velocity resulting from higher temperatures in the system. They postulated that this process is endothermic in nature, thereby it could be considered as a chemical adsorption process. Gusain et al. (2019) investigated adsorption of Pb^{2+} and Cd^{2+} ions from industrial mine using hierarchical MoS_2/SH-MWCNT nanocomposite and observed a similar trend which they attributed to an endothermic adsorption process and increased mobility of metal ions with an increase in temperature due to an increase in thermal energy of the system. They also added that an increase in temperature reduced the required activation energy by opening the MWCNT network structure as well as increasing the deprotonation of functional groups leading to additional binding sites. Mohammadifard and Amiri (2017) investigated the removal of Cu^{2+} ions from aqueous solutions using novel synthesized $CaCO_3$ nanoparticles prepared in a colloidal gas aphron and observed an increase in adsorption efficiency

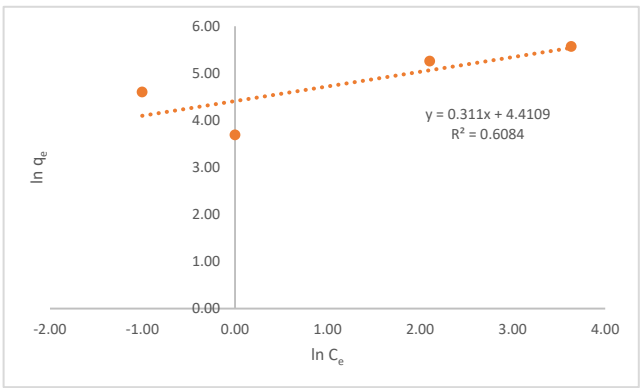

Figure 8. Linearized plot for the Freundlich isotherm model.

with an increase in temperature. They argued that this was in contradiction with what should happen with ordinary adsorption process behaviour which normally should be exothermic, thereby decreasing with an increase in temperature. However, this contradiction which was observed by other researchers mentioned above as well further gives evidence that the adsorption process is not just a "simple adsorption process".

El-Naggar et al. (2019) studied the removal of Pb^{2+} ions from wastewater using a natural composite adsorbent called Kaolinite/Smectite. They observed that increasing temperature increases adsorption capacity. They attributed this trend to an increase in reaction rate due to increased average velocity and diffusion of ions as they adhere onto the surface of the adsorbent. Our experimental results show that there is a positive correlation between adsorption efficiency and temperature in the range 27–60 °C. We elucidate that the adsorption process was indeed endothermic hence chemisorption as similarly observed by El-Naggar et al. (2019) and other investigators mentioned above.

Li et al. (2020) investigated adsorption of Hg^{2+} ions from aqueous solutions using thiol functionalized cobalt ferrite magnetic mesoporous silica composite and found an inverse relationship between temperature and adsorption efficiency which they attributed to weakening of bonds between cations and adsorption sites as temperature increased. Fathy et al. (2019) observed an inverse relationship between adsorption efficiency and temperature when they were investigating adsorption of Pb^{2+} and Co^{2+} ions using $CaCO_3$/HPC core-shell composite from aqueous solutions. They reasoned that the adsorption process was exothermic for both ions. They suggested further that increasing the temperature should weaken the physical or chemical attractive forces thereby reducing the sorbent ability.

Researchers have found the adsorption of Pb^{2+} ions onto adsorbents to be either endothermic as in our case or exothermic as in other cases. The endothermic nature of our process can be attributed to reduced desorption and an increase in adsorption sites as temperature is increased. This can be backed up by a steep increase in adsorption capacity and efficiency when temperature was increased from room temperature (27 °C) to 40 °C. However, the increase was lower above 40 °C, showing the initial impact of adding heat to move above the room temperature.

3.2.2. *Effect of initial sorbate concentration*

The relationship between the equilibrium values of the sorbate concentration (C_e) and the adsorption capacity (q_e) is given in Table 5 while Table 6 gives the summary of the results for different initial metal concentration. Figure 5 gives the adsorption isotherm for Pb^{2+} onto NSHS and Table 7 shows p-values from statistical analysis using ANOVA for C_e values in triplet, and using t-test for C_e, q_e and %R values.

Table 7 indicates that the means for C_e values range from a low of 3.78 to a high of 17.125 showing that our means are not very close from ANOVA analysis. The p-value we determined is 0.6163 which is greater than our significance level of 0.05. We accept the null hypothesis that our sample data provide strong evidence to conclude that the three C_e values for each of the initial metal ion concentration can be considered to be equal. This gives us the confidence that the average values we calculated and used in our calculations are a representative of the actual experimental results obtained. From t-test analysis, the mean for the actual and standard values for C_e, q_e and %R are 15.46 versus 0, 184.54 versus 200 and 0.94 versus 1, respectively. Our p-values for C_e, q_e and %R are all greater than the confidence level of 0.05 and therefore we accept the null hypothesis as our sample data support the hypothesis that there is no significant difference between our calculated values of C_e, q_e and %R and their standard values.

Figure 5 shows that there is a positive correlation between concentration of Pb^{2+} ions and q_e. This is because increased amount of Pb^{2+} ions will be available at a higher initial ion concentration, increasing the possibility of contact between the ions and the adsorbent (Lei et al.,

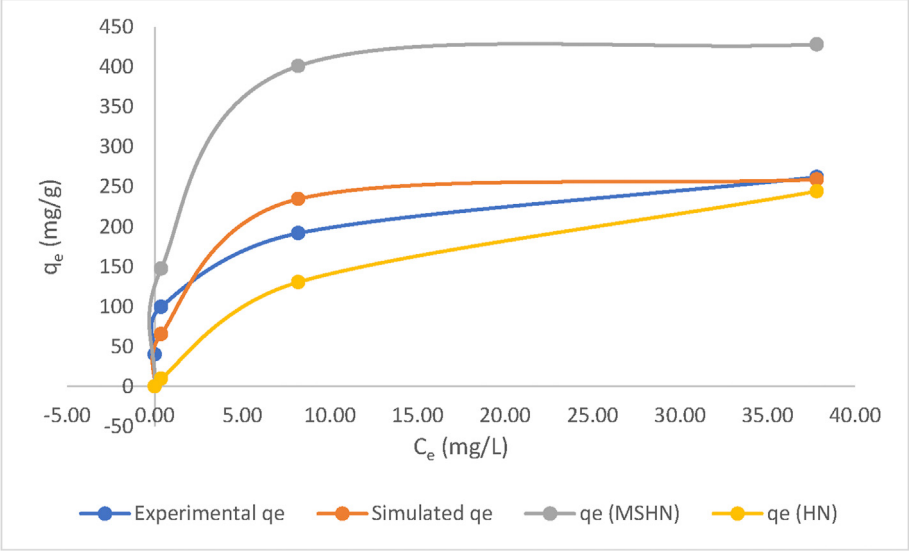

Figure 9. Langmuir isotherm from experimental and simulated data.

2019). In addition, a high initial metal ion concentration enhances diffusion from the solution to the adsorbent's active sites i.e. there is an increase in the diffusion gradient leading to an increase in the mass transfer process (Lei et al., 2019).

In general, our experimental results elucidate that there is a positive correlation between the initial metal ion concentration and adsorption capacity. In this study, we also observed that the adsorption efficiency decreased with an associated increase in initial metal ion concentration. At low initial concentration, all of the Pb^{2+} ions were successfully adsorbed (40–100 mg/g) of the adsorbent, proving that indeed at low concentrations the adsorbent is very effective and efficient. Fathy et al. (2019) observed a similar trend when investigating adsorption of Pb^{2+} and Co^{2+} ions using $CaCO_3$/HPC core-shell composite from aqueous solutions. They reasoned that at high initial metal concentrations there was increased competitive dispersion of metal ions at the adsorbent surface i.e. the pores of the adsorbent were closed and metal ions found it difficult to pass deep into the adsorbent pores, restricting adsorption to occur only on the adsorbent surface. This meant that if the adsorbent sites were reduced there was reduced adsorption efficiency. Mustapha et al. (2019) observed a similar trend in their adsorption experiments of Pb^{2+}, Cd^{2+}, Zn^{2+} and Cu^{2+} ions using *Albizia lebbeck* pods from aqueous solutions for initial metal concentration of 10–30 mg/L. They reasoned that when the initial concentration is increased, enhanced driving force between the solid and liquid phases results in saturation of the adsorption sites. We attribute this kind of behaviour to depletion of active sites on the surface of NSHS. However, when the initial concentration is lower, the trend reverses (Mustapha et al., 2019). Gusain et al. (2019) investigated adsorption of Pb^{2+} and Cd^{2+} ions from industrial mine while using hierarchical MoS_2/SH-MWCNT nanocomposite synthesized using a facile hydrothermal method and observed a slight decrease in adsorption efficiency with an increase in initial metal concentration for Pb^{2+} ions but a bigger decrease for Cd^{2+} ions. They attributed this observation to a decrease in binding sites with an increase in initial metal ion concentration due to saturation of the binding sites. El-Naggar et al. (2019) observed a similar trend when they employed a Kaolinite/Smectite natural composite adsorbent to study the removal of Pb^{2+} ions from wastewater, using different concentrations of Pb^{2+} ions ranging from 125 to 500 mg/L Lei et al. (2019) also observed a similar trend when using dopamine-modified magnetic nano-adsorbents to adsorb Cd^{2+} ions from an aqueous solution.

A plot of adsorbed metal ions per adsorbent (q_e) versus equilibrium concentration (C_e) is given in Figure 6 and it helped to explain our trend. Figure 6 shows that as the equilibrium concentration of Pb^{2+} ions is increased initially but the rate of adsorption at equilibrium plateaus i.e. the trend is levelling out. This is due to reduction of binding sites available for adsorption as initial metal ion concentration increases. This helps to explain our trend which shows that the rate of adsorption decreases with an increase in initial metal ion concentration (C_o). Higher C_o led to a higher C_e, leading to reduced rate of adsorption (q_e). In addition, higher C_e led to low q_e based on Eq. (5) and this is because of fixed binding sites available but now there is increased Pb^{2+} ions in solution with limited sites to bind to as the adsorbent mass was kept constant at 50 mg.

3.2.3. Adsorption isotherms

The two adsorption isotherms we considered during our studies were the Langmuir and the Freundlich isotherms. Results for the Langmuir isotherm model are given in Figure 7 and those for the Freundlich isotherm model are given in Figure 8.

Figure 7 shows a plot obtained from application of Eq. (2) while Figure 8 results from application of Eq. (4). From the regression analysis, the line of best fit for the plots gave correlation coefficients (R^2) values of 0.9937 and 0.6084 for Langmuir and Freundlich isotherms, respectively. A comparison with the coefficient of correlation for the Freundlich model, with a value of 0.6098 shows that the best model to describe the adsorption of Pb^{2+} on NSHS is the Langmuir isotherm. This suggests that the adsorption of Pb^{2+} ions on NSHS occurs on a homogeneous surface by a single layer (El-Naggar et al., 2019; Mustapha et al., 2019). A correlation coefficient of 0.6098, in comparison with that of the Langmuir, shows a poor fit implying that the Freundlich isotherm cannot be used to model the equilibrium relationship between adsorption capacity and sorbate concentration for the adsorption of Pb^{2+} ions on NSHS i.e. adsorption is not on a heterogeneous surface.

In this study, we used the Langmuir isotherm to best describe the adsorption equilibrium and we made use of Figure 7 and Eq. (2), to determine the parameters for Langmuir (b and q_m). We substituted the gradient and intercept values into some Eq. (2) to determine q_m and b, respectively and we determined $q_m = 266.89$ mg/g and $b = 0.89$ L/mg. The Langmuir isotherm for Pb^{2+} ions adsorption from wastewater using NSHS is given as:

$$q_{e(NSHS)} = \frac{236.96C_e}{1 + 0.89C_e} \tag{13}$$

A plot of q_e versus C_e for calculated q_e from Langmuir equation

Table 8. Comparison of different adsorption capacities of metal ions from aqueous solutions based on Langmuir adsorption isotherm.

Sample	Metal ion adsorbed	q_m (mg/g)	b (L/mg)	Contact time (mins)	Reference
Novel synthesized $CaCO_3$ nanoparticles	Cu^{2+}	666.67	0.1293	120	Mohammadifard and Amiri (2017)
Magnesium silicate hierarchical nanostructures	Pb^{2+}	436.68	1.3880	1440	Huang et al. (2017)
Hydroxyapatite nanostructures	Pb^{2+}	322.60	0.0830	80	Safatian et al. (2019)
NSHS	Pb^{2+}	266.89	0.8900	40	Present work
Thiol-functionalized cobalt ferrite magnetic mesoporous silica composite (SH-mSiO_2@$CoFe_2O_4$)	Hg^{2+}	258.80 (No model used)	-	180	Li et al. (2020)
Jujube Pit Biochar	Pb^{2+}	192.00	0.0036	30	Gao et al. (2020)
Hierarchical MoS_2/SH-MWCNT nanocomposite	Pb^{2+}	90.00 (Freundlich isotherm)	-	60	Gusain et al. (2019)
$CaCO_3$/HPC core-shell composite	Pb^{2+}	82.99	0.5119	150	Fathy et al. (2019)
Hierarchical MoS_2/SH-MWCNT nanocomposite	Cd^{2+}	66.67 (Freundlich isotherm)	-	60	Gusain et al. (2019)
Dopamine-modified magnetic nano-adsorbent	Cd^{2+}	21.58	0.0397	100	Lei et al. (2019)
Cashew nutshell adsorbent	Pb^{2+}	17.82	0.2197	30	Kumar, 2014
Albizia lebbeck pods	Pb^{2+}	7.17	0.4300	30	Mustapha et al. (2019)
Kaolinite/Smectite-B clay	Pb^{2+}	6.51	0.2700	120	El-Naggar et al. (2019)
Kaolinite/Smectite-A clay	Pb^{2+}	5.84	0.1620	120	El-Naggar et al. (2019)
$CaCO_3$/HPC core-shell composite	Co^{2+}	3.47 (Freundlich isotherm)	-	150	Fathy et al. (2019)

against experimental q_e shows good estimation using the equation (Figure 9).

Huang et al. (2017) investigated adsorption of Pb^{2+}, Zn^{2+} and Cu^{2+} ions from aqueous solution using magnesium silicate hierarchical nanostructures and determined that adsorption of Pb^{2+}, Zn^{2+} and Cu^{2+} ions were best modelled by Langmuir isotherm ($R^2 = 0.999$) with maximum adsorption capacity of 436.68, 78.86 and 52.30 mg/g, respectively. Safatian et al. (2019) investigated the adsorption of Pb^{2+} ions from water and wastewater using hydroxyapatite nanostructures that were synthesized from eggshells using microwave irradiation. Their adsorption process was better modelled using the Langmuir isotherm ($R^2 = 0.994$). Fathy et al. (2019) investigated the adsorption of Pb^{2+} and Co^{2+} ions using $CaCO_3$/HPC core-shell composite from aqueous solutions and observed that the adsorption process for Pb^{2+} ions was better modelled with Langmuir isotherm ($R^2 \geq 0.930$) but the adsorption of Co^{2+} was better modelled by Freundlich isotherm ($R^2 \geq 0.900$). Mustapha et al. (2019) observed that the Langmuir isotherm better fitted adsorption of Pb^{2+} ions from aqueous solutions when using *Albizia lebbeck* pods, however, Cd^{2+}, Zn^{2+} and Cu^{2+} ions could be modelled by either the Langmuir or the Freundlich isotherm from the same experimental studies.

Gusain et al. (2019) investigated adsorption of Pb^{2+} and Cd^{2+} ions using hierarchical MoS_2/SH-MWCNT nanocomposite and the adsorption was better modelled using the Freundlich isotherm for both metal ions indicating chemisorption i.e. multilayer adsorption of metal ions on heterogeneous surfaces. El-Naggar et al. (2019) noticed that the adsorption of Pb^{2+} ions from wastewater using Kaolinite/Smectite natural composite adsorbents followed Freundlich isotherm based on correlation coefficient values, unlike Langmuir isotherm for this study. Gao et al. (2020) observed that the adsorption of Pb^{2+} ions from wastewater using biochar adsorbent obtained from jujube pit followed Freundlich isotherm based on correlation coefficient values.

The majority of the studies using different adsorbents for adsorption of Pb^{2+} ions from aqueous solutions modelled the adsorption process using the Langmuir adsorption isotherm. This gives further evidence that the adsorption process was homogeneous by a single layer and it was not chemisorption controlled. In Table 8, we illustrate the differences in performance of various adsorbents in terms of their adsorption capacities for lead ions.

From Table 8, the performance of NSHS was found to be very competitive and favourable in comparison to other adsorbents. The other adsorbents that outshone ours were nano based showing the impact of nanomaterials in adsorption process. The NSHS adsorbent has one of the largest intensity of adsorption and the highest amount of metal ions per unit mass of adsorbent that forms a complete surface monolayer. The high adsorption capacity for NSHS and other nano-based materials can be attributed to their higher surface area to volume ratio as alluded to earlier. In addition to this, the high adsorption capacity and efficiency of NSHS supported on $CaCO_3$ can partly be attributed to the polymorph and size of the applied $CaCO_3$ particles which can assist with adsorption of Pb^{2+} ions from aqueous solution. These results show that the NSHS we synthesized in this investigation is capable of removing lead ions from wastewater competitively.

In addition, the NSHS had very high maximum adsorption rates (q_m) and Langmuir adsorption equilibrium constant (b). The high q_m and b makes NSHS superior as the equations for determining q_e for adsorbents on Pb^{2+} ions higher than NSHS in Table 8 were $q_{e(MSHN)} = \frac{606.11C_e}{1+1.3884C_e}$ and $q_{e\ (HN)} = \frac{26.75C_e}{1+0.083C_e}$ which were plotted on Figure 9. The plots show that only adsorption using magnesium silicate hierarchical nanostructures (MSHN) gave better results than NSHS while adsorption using hydroxyapatite nanostructures (HN) had lower q_e values for the same equilibrium concentration range from our study. This shows that NSHS nanoparticles are able to compete successfully with other adsorbents being synthesized to remove Pb^{2+} ions from aqueous solutions.

We then used Eq. (14) and the Langmuir isotherm parameters to evaluate the affinity between the adsorbent and adsorbate through a dimensionless separation factor, R_L.

$$R_L = \frac{1}{1 + bC_o} \tag{14}$$

The R_L values makes it easy to determine whether the adsorption is irreversible ($R_L = 0$), favorable ($0 < R_L < 1$), linear ($R_L = 1$) or unfavourable ($R_L > 1$) (Mustapha et al., 2019). In Table 9 we show the calculated values of R_L for all the different initial metal ion concentrations.

The R_L values showed that the adsorption is favourable for all initial metal ion concentrations. Table 9 reveals that there is a negative correlation between R_L and metal ion concentration, which implies enhanced adsorption of ions at lower initial metal ion concentrations. This gave further evidence to support observation of a reduction in adsorption efficiency/rate with an increase in initial metal ion concentration.

3.2.4. Adsorption thermodynamics

To determine the thermodynamic parameters, we plotted ln K_p versus 1/T (K^{-1}) from Table 3 and the results are shown in Figure 10.

We then performed a regression analysis and determined the correlation coefficient to be 0.8787. The corresponding equation of the line of best fit gave a gradient of -11698, corresponding to $-\frac{\Delta H^o}{R}$ and an intercept

Table 9. Separation factors for the adsorption of Pb^{2+} ions from wastewater using NSHS.

Initial concentration (mg/L)	40	100	200	300
R_L	0.0274	0.0111	0.0056	0.0037

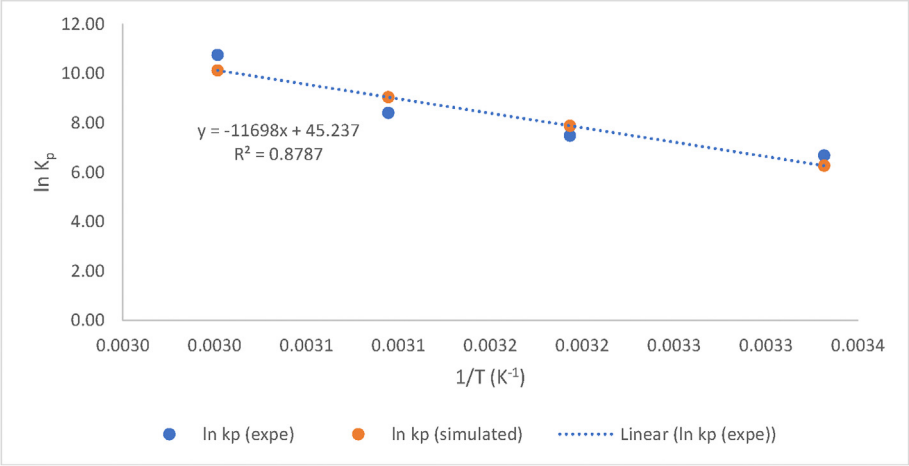

Figure 10. Relationship between the inverse of temperature and the adsorption equilibrium constant.

of 45.237 corresponding to $\frac{\Delta S^o}{R}$. Therefore, using Eqs. (10) and (11), the thermodynamic parameters were determined as follows: $\Delta H = 97.255$ kJ/mol, $\Delta S = 0.376$ kJ/mol·K and $\Delta G = -22.120$ kJ/mol. These three values show that the adsorption process for Pb^{2+} ions on NSHS is endothermic as evidenced by a positive ΔH value; and spontaneous as evidenced by a negative ΔG value. ΔH° values for adsorption can be used to determine whether the process is physical ($2 < \Delta H^o < 21$ kJ/mol), physico-chemical ($21 < \Delta H^o < 80$ kJ/mol) or chemical ($80 < \Delta H^o < 200$ kJ/mol) adsorption (Lei et al., 2019). This means that adsorption was of the chemisorption type due to a ΔH^o value that lies in the range 80–200 kJ/mol. The positive ΔS value indicates that Pb^{2+} ions in the bulk aqueous phase/solution are in a state of disorder as compared to the relatively orderly state on the adsorbent's surface. However, the lower value of ΔS indicate that the ions are moving towards the ordered nature on the adsorbent surface.

The values of ΔG at the various temperatures were negative. We also observe that there is a negative correlation between ΔG and the solution temperature, which show that the adsorption process of Pb^{2+} ions on NSHS was enhanced at higher temperatures i.e. the degree of spontaneous reaction increases with an increase in temperature (Mustapha et al., 2019). The comparison between the thermodynamic data of NSHS and other adsorbents is summarised in Table 10.

Again, NSHS adsorbents are showing good performance against other adsorbents by giving higher thermodynamic values. This is proving their worth in removing Pb^{2+} ions from aqueous solutions. The activation energy and activity constant were determined using Arrhenius law, Eq. (16) and Figure 10 (El-Aila et al., 2016).

$$K_p = Ae^{-\frac{E_a}{RT}} \tag{15}$$

Taking natural logarithms:

$$\ln K_p = \ln A - \frac{E_a}{RT} \tag{16}$$

where K_p is adsorption equilibrium constant, A is pre-exponential constant, E_a is activation energy for the reaction (kJ/mol), R is ideal gas constant (kJ/mol·K) and T is absolute temperature (K).

Using the same gradient and intercept, the activation energy (E_a) was found to be 97.255 kJ/mol and pre-exponential constant was found to be 4.43×10^{19}. Therefore the Arrhenius law for adsorption of Pb^{2+} ions from wastewater using NSHS is given by:

$$K_p = 4.43x10^{19} \times e^{\left(\frac{-11697.75}{T(K)}\right)} \tag{17}$$

Table 10. Differences in thermodynamic data for adsorption capacities of Pb^{2+} from wastewater between NSHS and other adsorbents.

Sample	Metal ion adsorbed	ΔH^o (kJ/mol)	ΔS^o (J/mol·K)	ΔG^o (kJ/mol)	Average T (°C)	Reference
Kaolinite/Smectite-B clay	Pb^{2+}	2.18×10^7	79.00	-6700	53	El-Naggar et al. (2019)
NSHS	Pb^{2+}	97.255	376.10	-22.120	44	Present work
$CaCO_3$/HPC core-shell composite	Pb^{2+}	41.912	90.68	-15.034	42.5	Fathy et al. (2019)
Albizia lebbeck pods	Pb^{2+}	33.161	94.49	2.641	55	Mustapha et al. (2019)
Dopamine-modified magnetic nano-Adsorbent	Cd^{2+}	25.714	0.13	-14.847	33	Lei et al. (2019)
Jujube Pit Biochar	Pb^{2+}	22.520	170.00	-29.85	30	Gao et al. (2020)
Hierarchical MoS_2/SH-MWCNT nanocomposite	Pb^{2+}	8.06	54.30	-8.66	40	Gusain et al. (2019)
Kaolinite/Smectite-A clay	Pb^{2+}	0.015	28.30	-584	53	El-Naggar et al. (2019)
Cashew nutshell adsorbent	Pb^{2+}	-5.607	-7.96	-3.112	45	Kumar, 2014

This is the Arrhenius law for Pb^{2+} ions adsorption using NHSH from wastewater. Mustapha et al. (2019) determined the activation energy of 33.161 kJ/mol when using *Albizia lebbeck* pods to remove metal ions include lead from aqueous solutions. The performance of NSHS on adsorption of Pb^{2+} ions can be seen plotted on Figure 10 for the simulated equation. The estimate is very good within the temperature range.

4. Conclusion

In this equilibrium and thermodynamic investigation, we successfully synthesized nano silica hollow spheres (NSHS) that were verified by the three characterization techniques employed. We then used the synthesized NSHS particles to remove Pb^{2+} ions from wastewater. From our experimental results, we can conclude that temperature and initial metal ion concentration affect the adsorption of Pb^{2+} ions onto NSHS. We elucidated that the Langmuir model best describes the relationship between adsorption capacity at equilibrium and the corresponding sorbate concentration which means that it was monolayer and physical adsorption. We also concluded that the optimum adsorption capacity of NSHS for Pb^{2+} ions was 266.89 mg/g. We discovered from our experimental results that the adsorption of Pb^{2+} ions from wastewater onto the adsorbent surface was monolayer and homogeneous. We concluded that the removal of Pb^{2+} ions using NSHS is an endothermic adsorption process characterised by a positive correlation between adsorption capacities, implying that it was a chemisorption adsorption process from ΔH value. We also noted a negative correlation between adsorption of Pb^{2+} ions onto NSHS sites and their initial metal ion concentration. The thermodynamic parameter, ΔH^o was a positive value, showing that it was an endothermic process. On the same note, the adsorption process was also found to be spontaneous, as given by the corresponding negative ΔG^o value. In conclusion, we would like to summarise our results by pointing out that the NSHS possesses good adsorption abilities for Pb^{2+} ions from wastewater and we infer that these nano particles can be used for industrial scale applications to remove Pb^{2+} ions.

In future, there is need to test the nanomaterial, NSHS on its suitability for the removal of various other heavy metals such as chromium and arsenic. In the current study, the adsorption process was batch-wise, so an in-depth study using continuous systems is highly recommended. This is because continuous systems give a more realistic resemblance to the industrial setup. In addition, desorption and reusability test experiments should be conducted to reduce the cost of the adsorbent as it will be more attractive if it can be used more than once.

Declarations

Author contribution statement

Milton Manyangadze: Conceived and designed the experiments; Performed the experiments; Analyzed and interpreted the data; Contributed reagents, materials, analysis tools or data; Wrote the paper.

Nyaradzai M.H. Chikuruwo, Gratitude Charis, Gwiranai Danha & Tirivaviri A. Mamvura: Analyzed and interpreted the data; Contributed reagents, materials, analysis tools or data; Wrote the paper.

T. Bala Narsaiah & Ch. Shilpa Chakra: Conceived and designed the experiments; Analyzed and interpreted the data; Contributed reagents, materials, analysis tools or data; Wrote the paper.

Funding statement

The authors would like to acknowledge their individual institutions for assisting with the study. The institutions are Chemical and Process Systems Engineering Department, Harare Institute of Technology, Harare, Zimbabwe; Industial and Manufacturing Engineering Department, Harare Institute of Technology, Harare, Zimbabwe; Institute of Chemical Sciences and Technology, Jawaharlal Nehru Technological University, Hyderabad, India and Department of Chemical, Materials and Metallurgical Engineering, College of Engineering and Technology, Botswana International University of Science and Technology, Botswana.

Competing interest statement

The authors declare no conflict of interest.

Additional information

No additional information is available for this paper.

References

Badruddoza, A.Z.Md., Shawon, Z.B.Z., Rahman, Md.T., Hao, K.W., Hidajat, K., Uddin, M.S., 2013. Ionically modified magnetic nanomaterials for Arsenic and Chromium removal from water. Chem. Eng. J. 225, 607–615.

Bonamente, M., 2017. Statistics and Analysis of Scientific Data. Springer-Verlag, New York, USA.

Chen, J.F., Ding, H.M., Wang, J.X., Shao, L., 2004. Preparation and characterization of porous hollow silica nanoparticles for drug delivery application. Biomaterials 25, 723–727.

Dekking, F.M., Kraaikamp, C., Lopuhaä, H.P., Meester, L.E., 2005. A Modern Introduction to Probability and Statistics: Understanding Why and How. Springer-Verlag, London, UK.

El-Aila, H.J., Elsousy, K.M., Hartany, K.A., 2016. Kinetics, equilibrium, and isotherm of the adsorption of cyanide by MDFSD. Arab. J. Chem. 9, S198–S203.

El-Naggar, I.M., Ahmed, S.A., Shehata, N., Sheneshen, E.S., Fathy, M., Shehata, A., 2019. A novel approach for the removal of lead (II) ion from wastewater using Kaolinite/Smectite natural composite adsorbent. Appl. Water Sc. 9, 7.

Fathy, M., Zayed, M.A., Moustafa, Y.M., 2019. Synthesis and applications of $CaCO_3$/HPC core–shell composite subject to heavy metals adsorption processes. Heliyon 5, e02215.

Gao, J., Liu, Y., Li, X., Yang, M., Wang, J., Chen, Y., 2020. A promising and cost-effective biochar adsorbent derived from jujube pit for the removal of Pb(II) from aqueous solution. Sci. Rep. 10, 7473.

Gusain, R., Kumar, N., Fosso-Kankeu, E., Ray, S.S., 2019. Efficient removal of Pb(II) and Cd(II) from industrial mine water by a hierarchical MoS_2/SH-MWCNT nanocomposite. ACS Omega 4, 13922–13935.

Hao, S., Zhong, Y., Pepe, F., Zhu, W., 2012. Adsorption of Pb^{2+} and Cu^{2+} on anionic surfactant-templated amino-functionalized mesoporous silica. Chem. Eng. J. 189–190, 160–167.

Huang, S.H., Chen, D.H., 2009. Rapid removal of heavy metal cations and anions from aqueous solutions by an amino-functionalized magnetic nano-adsorbent. J. Hazard. Mater. 163, 174–179.

Huang, R., Wu, M., Zhang, T., Li, D., Tang, P., Feng, Y., 2017. Template-free synthesis of large-pore-size porous magnesium silicate hierarchical nanostructures for high-efficiency removal of heavy metal ions. ACS Sustain. Chem. Eng. 5 (3), 2774–2780.

Kegl, T., Ban, I., Lobnik, A., Košak, A., 2019. Synthesis and characterization of novel γ-Fe_2O_3-NH_4OH@SiO_2(APTMS) nanoparticles for dysprosium adsorption. J. Hazard Mater. 378.

Kegl, T., Košak, A., Lobnik, A., Novaka, Z., Kovač Kralj, A., Ban, I., 2020. Adsorption of rare earth metals from wastewater by nanomaterials: a review. J. Hazard Mater. 386.

Kumar, P.S., 2014. Adsorption of lead(II) ions from simulated wastewater using natural waste: a kinetic, thermodynamic and equilibrium study. Environ. Prog. Sustain. Energy 33 (1), 55–64.

Lei, T., Li, S.-J., Jiang, F., Ren, Z.-X., Wang, L.-L., Yang, X.-J., Tang, L.-H., Wang, S.-X., 2019. Adsorption of cadmium ions from an aqueous solution on a highly stable dopamine-modified magnetic nano-adsorbent. Nanoscale Res. Lett. 14, 352.

Li, K., Xie, L., Hao, Z., Xiao, M., 2020. Effective removal of Hg(II) ion from aqueous solutions by thiol functionalized cobalt ferrite magnetic mesoporous silica composite. J. Dispersion Sci. Technol. 41 (4), 503–509.

Manyangadze, M., Govha, J., Narsaiah, B.T., Kumar, P., Chakra, Ch.P.S., 2017. Removal of Pb^{2+} from Water Using Silica Nano Spheres Synthesized on $CaCO_3$ as a Template – Adsorption Kinetics, Innovative Technologies for the Treatment of Industrial Wastewater: A Sustainable Approach. Apple Academic Press Publications, New Jersey, USA.

Misran, H., Yarmo, M.A., Ramesh, S., 2013. Synthesis and characterization of silica nanospheres using nonsurfactant template. Ceram. Int. 39, 931–940.

Mohammadifard, H., Amiri, M.C., 2017. Evaluating Cu(II) removal from aqueous solutions with response surface methodology by using novel synthesized $CaCO_3$ nanoparticles prepared in a colloidal gas aphron system. Chem. Eng. Commun. 204 (4), 476–484.

Mourhly, A., Khachani, M., El Hamidi, A., Kacimi, M., Halim, M., Arsalane, S., 2015. The synthesis and characterization of low-cost mesoporous silica SiO_2 from local pumice rock. Nanomater. Nanotechnol. 5, 35.

Mustapha, S., Shuaib, D.T., Ndamitso, M.M., Etsuyankpa, M.B., Sumaila, A., Mohammed, U.M., Nasirudeen, M.B., 2019. Adsorption isotherm, kinetic and thermodynamic studies for the removal of Pb(II), Cd(II), Zn(II) and Cu(II) ions from aqueous solutions using *Albizia lebbeck* pods. Appl. Water Sci. 9, 142.

Musić, S., Filipović-Vinceković, N., Sekovanić, L., 2011. Precipitation of amorphous SiO_2 particles and their properties. Braz. J. Chem. Eng. 28 (1), 89–94.

Quirk, T.J., 2014. Excel 2010 for Engineering Statistics: A Guide to Solving Practical Problems. Springer, Cham, Switzerland.
Safatian, F., Doago, Z., Torabbeigi, M., Shams, H.R., Ahadi, N., 2019. Lead ion removal from water by hydroxyapatite nanostructures synthesized from egg sells with microwave irradiation. Appl. Water Sci. 9, 108.
Sayago, U.F.C., Castro, Y.P., Rivera, L.R.C., Mariaca, A.G., 2020. Estimation of equilibrium times and maximum capacity of adsorption of heavy metals by *E. crassipes* (review). Environ. Monit. Assess. 192, 141.
Singh, S., Barick, K.C., Bahadur, D., 2013. Functional Oxide nanomaterials and nanocomposites for the removal of heavy metals and dyes. Nanomater. Nanotechnol. 3–20. InTech.
Singh, S., Barick, K.C., Bahadur, D., 2011. Surface engineered magnetic nanoparticles for removal of toxic metal ions and bacterial pathogens. J. Hazard Mater. 192, 1539–1547.
Zulfiqar, U., Subhani, T., Wilayat Husain, S., 2016. Synthesis and characterization of silica nanoparticles from clay. J. Asian Ceram. Soc. 4 (1), 91–96.